JOURNAL OF SOLID STATE CHEMISTRY **139,** 161–167 (1998)
ARTICLE NO. SC987826

Amorphization of $Ca_3(VO_4)_2$ at High Pressure

Andrzej Grzechnik

École Normale Supérieure de Lyon, 46, allée d'Italie, 69364 Lyon Cedex 07, France

Received July 25, 1997; in revised form March 16, 1998; accepted March 24, 1998

The combined X-ray diffraction and Raman spectroscopy data show that $Ca_3(VO_4)_2$ irreversibly amorphizes at 10.0 GPa and room temperature. The amorphization, with its onset at about 8.5 GPa, is not preceded by any phase transition in the crystalline phase, which possesses highly anisotropic compressibility (the axial stiffness along the *a* axis is over 30% larger than the axial stiffness along the *c* axis). The results of Raman spectroscopy measurements demonstrate that structural rearrangements in the amorphous $Ca_3(VO_4)_2$ occur between 8.1 and 14.8 GPa. This is associated with a large deformation of the VO_4^{3-} units or the increase of the average coordination number for the V^{5+} cations in the amorphous material. A large hysteresis of this phase change is observed upon decompression, suggesting a first-order character of polymorphic transitions within the amorphous material.

INTRODUCTION

Calcium orthovanadate, $Ca_3(VO_4)_2$, is a high-temperature ferroelectric ($T_c = 1383$ K) (1–4) with additional anomalies in pyroelectric and dielectric properties (1) and electronic thermal emission spectra (3) at the 550–800 K temperature range. When activated with rare-earth elements, $Ca_3(VO_4)_2$ exhibits intense luminescence and can be used as a luminophore and a host material for lasers (3, 5–7). Its luminescent properties are enhanced in solid solution series with other alkali earth orthovanadates (8) or phosphates (3). $Ca_3(VO_4)_2$ is also a possible host for Mn^{5+} in the $Ca_3(VO_4)_2:Mn^{5+}$ laser system (9). The defect structure of calcium orthovanadate along with the presence of V^{4+} ions or rare-earth doping accounts for its high electronic conductivity (10–12).

The structure of $Ca_3(VO_4)_2$ is related to the structure of $K_2Pb(SO_4)_2$, palmierite ($R\bar{3}m$, $Z = 1$), consisting of $[Pb(SO_4)_2]^{2-}$ layers linked into a crystal network by K^+ cations (13). The unit cell of $Ca_3(VO_4)_2$ is doubled along the *a* and *c* axes ($R3c$, $Z = 7$) as a result of displacements of oxygen and calcium atoms from their ideal positions (14). VO_4^{3-} tetrahedra occupy one C_3 and two C_1 sites, with different tilting perpendicular to the *c* axis. The coordination numbers of two nonequivalent $Ca_{(1)}^{2+}$ cations (corresponding to intralayer Pb^{2+} sites in the palmierite structure) are 6 and 8. Three nonequivalent $Ca_{(2)}$ atoms (corresponding to interlayer K^+ sites in the palmierite structure) are sixfold, sevenfold, and eightfold coordinated. The interlayer $Ca_{(2)}^{2+}$ at the C_3 sites are half occupied with a random distribution of vacancies. $Ca_3(VO_4)_2$ is isostructural with its phosphorus and arsenic analogues (14, 15). The ideal palmierite structure is taken by a whole family of $Me_3(XO_4)_2$ compounds (Me^{2+} = Sr, Ba, Pb; X^{5+} = P, As, V, Mn) at ambient conditions (16–18).

Pressure-induced structural changes in $Ba_3(VO_4)_2$ and $Sr_3(VO_4)_2$ were previously studied via Raman spectroscopy (19, 20). The spectral changes in $Ba_3(VO_4)_2$ were interpreted as being due to condensation of VO_4^{3-} units into edge- or corner-shared octahedra with little or no hysteresis on decompression. For $Sr_3(VO_4)_2$, there is a pressure-induced first-order phase change at about 15.0 GPa, with large hysteresis on decompression, which was rationalized as a transition into a spinelloid series of structures, retaining the tetrahedral coordination of the V atoms.

As the size of the intra- and interlayer cations decreases from Ba to Ca, the symmetry of the structure at ambient conditions is reduced from $R\bar{3}m$ to $R3c$ (14, 21, 22). The differences in the high-pressure behavior of $Ba_3(VO_4)_2$ and $Sr_3(VO_4)_2$ could be attributed to the relative size of the Ba^{2+} and Sr^{2+} cations (19, 20). $Ca_3(VO_4)_2$, disordered at ambient pressure, may be seen as an intermediate between amorphous and crystalline solids. It is of interest then to elucidate the possible pressure-induced structural changes in this compound and to compare them with the ones observed in $Ba_3(VO_4)_2$ and $Sr_3(VO_4)_2$. In this work, the effects of external pressure on the structure of calcium orthovanadate, $Ca_3(VO_4)_2$, are studied by X-ray diffraction and Raman spectroscopy in a diamond anvil cell.

EXPERIMENTAL

The polycrystalline sample of $Ca_3(VO_4)_2$ was prepared from a 3 : 1 mixture of $CaCO_3$ and V_2O_5 (both from Aldrich) melted and cooled to room temperature from 1900 K.

0022-4596/98 $25.00

X-ray diffraction patterns were recorded using an energy-dispersive configuration on the wiggler line of the DCI storage ring at the Laboratoire pour l'Utilization du Rayonnement Électromagnétique (LURE, Orsay, France). The polychromatic X-ray beam was collimated to a 100×100 μm sized spot on the pressurized sample. The diffracted beam was collected between 5 and 60 keV ($Ed = 50.27 \pm 0.03$ keV Å) using a Canberra planar germanium detector. The sample was loaded into a membrane diamond cell with type I diamonds, brilliant cut with 500 μm culets, and a sample chamber diameter of 250 μm. Silicone oil was used as a pressure transmitting medium.

Raman spectra were collected using an ISA S-3000 triple spectrograph and a Coherent Model 90-5 Ar^+ laser as the excitation source at a wavelength of 488 nm. An Olympus BH-2 petrographic microscope was used to collect both incident and scattered radiation in a backscattering geometry. A Princeton Instruments LN/CCD-1100 detector was used. The sample was loaded into a Mao-Bell-type diamond cell with type I diamonds, brilliant cut with 350 μm culets, and a sample chamber diameter of 150 μm. CsI was used as a pressure transmitting medium.

Pressures during both X-ray diffraction and Raman spectroscopy experiments were determined from the R_1 ruby fluorescence line (23). The estimated error in pressure measurements in both experiments did not exceed 3% of the measured value.

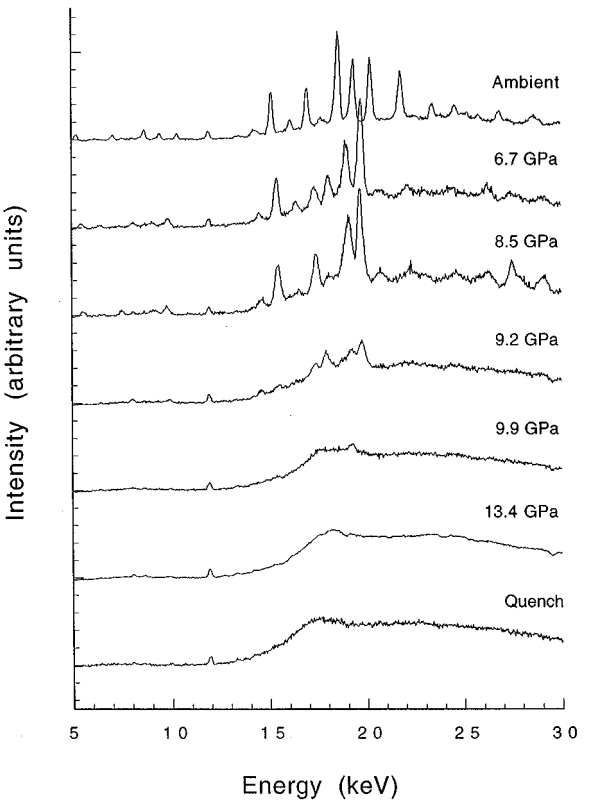

FIG. 1. Energy-dispersive X-ray diffraction patterns of $Ca_3(VO_4)_2$ as a function of pressure. The patterns are normalized to the intensity of the external impurity peak (without any pressure dependence) at about 11.94 keV.

RESULTS

X-Ray Diffraction

The energy-dispersive X-ray diffraction patterns of $Ca_3(VO_4)_2$ as a function of pressure are shown in Fig. 1. The pattern at ambient conditions can be indexed in the $R3c$ space group, in agreement with the reported crystal structure (14). As shown in Table 1, the overestimated c lattice parameter in this study leads to an overestimation of the unit cell volume by less than 1% relative to the value from the JCPDS-ICDD database. At low pressures up to 8.0 GPa, all diffraction peaks can be refined within the $R3c$ symmetry, indicating that there is no phase transition in $Ca_3(VO_4)_2$ in this pressure range (Figs. 2 and 3). At higher pressures, the X-ray diffraction peaks broaden, decrease in intensity, and entirely vanish above 10 GPa, signaling the appearance of a pressure-induced amorphous material. Upon further compression, only broad X-ray diffraction diffuse peaks, due to the $Ca_3(VO_4)_2$ amorphous material, are visible. The diffuse features, with no peaks due to crystalline phases, are also observed in the X-ray pattern of the sample decompressed from 13.4 GPa.

The obtained data on the pressure dependence of the lattice parameters up to 8.0 GPa were used to extract information on the compressibility of $Ca_3(VO_4)_2$. The pressure (P)–volume (V) data were fit to a third-order Birch–Murnaghan equation of state (EoS) (24)

$$P = \tfrac{3}{2} K_0 \left[(V_0/V)^{7/3} - (V_0/V)^{5/3}\right] \times \left\{1 + \tfrac{3}{4}(K_0' - 4)\left[(V_0/V)^{2/3} - 1\right]\right\}$$

to find the volume of the unit cell at zero pressure (V_0) and the isothermal bulk modulus (K_0) along with its K_0' first pressure derivative, both at zero pressure (Table 1 and Fig. 3). The modified Birch–Murnaghan equation of state was fit to the pressure (P)–a lattice parameter (a) and pressure (P)–c lattice parameter (c) data

$$P = \tfrac{1}{2}(1/\beta_a)\left[(a_0/a)^{7/3} - (a_0/a)^{5/3}\right]$$

and

$$P = \tfrac{1}{2}(1/\beta_c)\left[(c_0/c)^{7/3} - (c_0/c)^{5/3}\right]$$

to obtain the parameters of axial stiffness at zero pressure (a_0 and c_0 lattice parameters) and the $1/\beta_a$ and $1/\beta_c$ axial stiffness parameters (Table 1 and Fig. 2). In general, the inverse values of the K_0 and $1/\beta$ parameters are average volume and axial compressibilities, respectively.

TABLE 1
Lattice, Axial Stiffness, and Equation of State Parameters of $Ca_3(VO_4)_2$ at Ambient Conditions

Lattice	a (Å)	c (Å)	V (Å^3)
This study	10.822(9)	38.278(111)	3882.22(10.61)
JCPDS-ICDD 39-90	10.811(1)	38.025(3)	3848.86

Axial stiffness	a_0 (Å)	$1/\beta_a$ (GPa)	c_0 (Å)	$1/\beta_c$ (GPa)
	10.82(1)	1074.7(36.6)	38.20(4)	808.2(53.2)

Equation of state	V_0 (Å^3)	K_0 (GPa)	K'_0
	3876.8(5.1)	92.50(8.23)	5.89(2.38)
	3874.2(3.6)[a]	99.08(2.25)[a]	4.00[a]

[a] Results obtained with a constrained EoS fit with $K'_0 = 4.00$.

As shown in Table 1, the a_0, c_0, and V_0 parameters agree well with the corresponding refined lattice parameters of $Ca_3(VO_4)_2$ at ambient pressure. Also, a constrained EoS fit with $K'_0 = 4.00$ results in a value of the isothermal bulk modulus (the measure of bulk hardness) similar to the one from a fully relaxed third-order fit. This observation along with a good agreement of the modified equation-of-state fits to a pressure dependence of the a and c lattice parameters suggests that $Ca_3(VO_4)_2$ deforms almost linearly until it amorphizes at about 8.5 GPa and room temperature. Comparison of the $1/\beta_a$ and $1/\beta_c$ parameters, which are the measures of hardness along the a and c crystallographic axes, respectively, reveals that the axial stiffness along the a axis in $Ca_3(VO_4)_2$ is over 30% larger than the axial stiffness along the c axis.

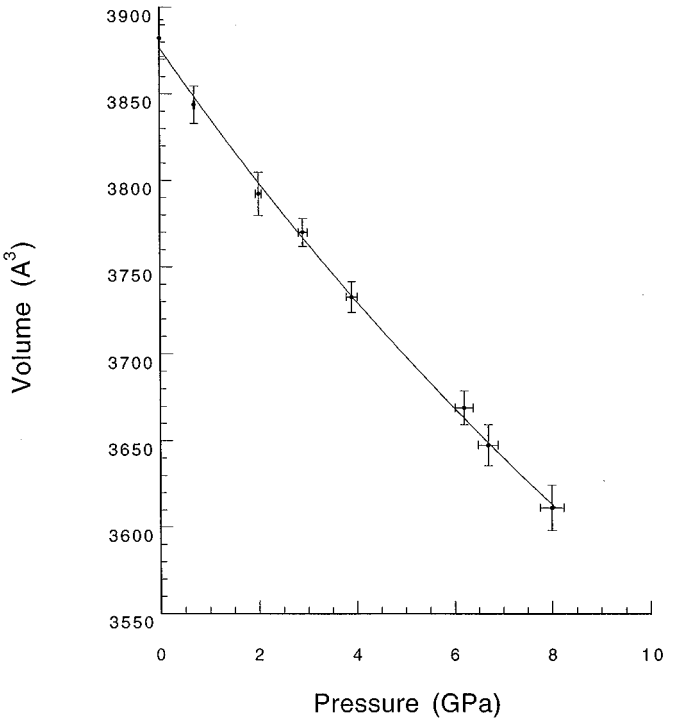

FIG. 3. Variation of the $Ca_3(VO_4)_2$ unit cell volume with pressure.

Raman Spectroscopy

Observed Raman bands in $Ca_3(VO_4)_2$ at zero pressure are distributed in two wavenumber regions corresponding to the V–O stretching modes (950–750 cm^{-1}) and O–V–O bending modes mixed with the translational and rotational modes of the VO_4^{3-} groups as well as Ca^{2+} cation

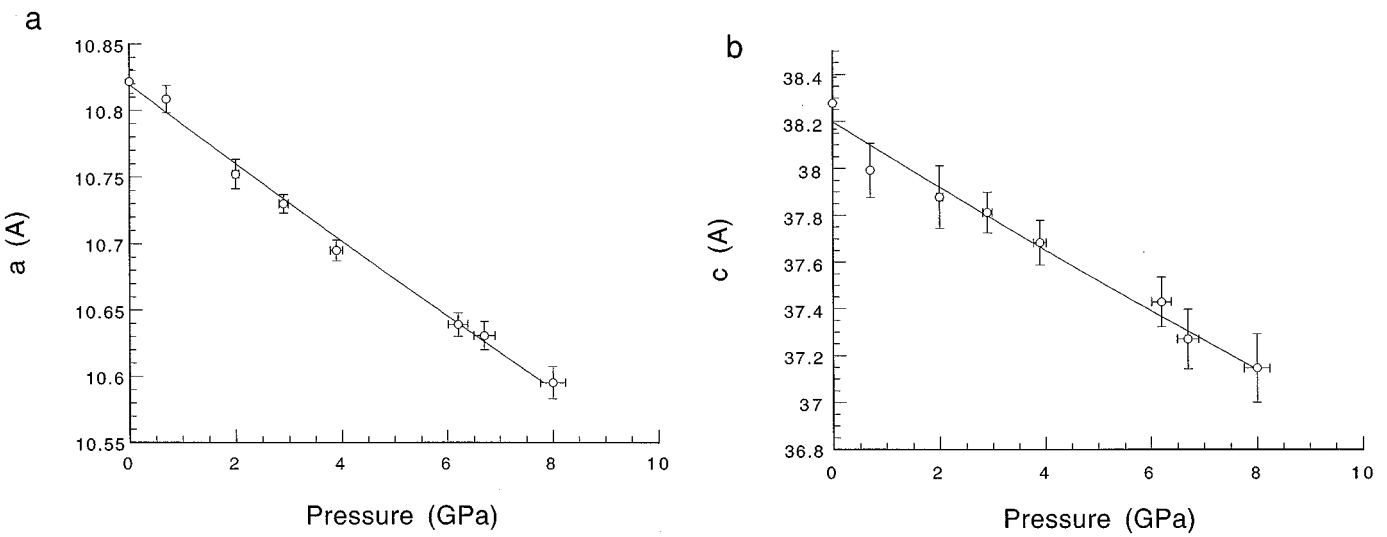

FIG. 2. Variation of the $Ca_3(VO_4)_2$ unit cell parameters with pressure: (a) the a parameter; (b) the c parameter.

displacements (450–50 cm^{-1}) (25). Up to 8.1 GPa, all the bands shift monotonously toward higher wavenumbers with no mode softening (Fig. 4). Such vibrational behavior in that pressure range is in agreement with the X-ray data, supporting the observation that there is no phase transition before the onset of amorphization at about 8.5 GPa and room temperature. The Raman spectrum recorded at 8.1 GPa still shows the spectral features of the crystalline form of $Ca_3(VO_4)_2$, although all the bands are considerably broader than the corresponding ones at lower pressures. Such broadening of the bands, i.e., disordering of the structure, is premonitory to amorphization at higher pressures. Upon further compression, the intense bands in both the 950–750- and 450–50-cm^{-1} regions can no longer be resolved. There also occurs a significant decrease in their intensity, due to the progressing amorphization of the material, as documented with X-ray diffraction (Fig. 1). It is remarkable that in the 8.1- to 14.8-GPa pressure range, the intense V–O stretching mode shows a negative pressure shift. At pressures above 14.8 GPa, this mode hardens and shifts toward higher wavenumbers. This indicates that the structural rearrangement in the amorphous $Ca_3(VO_4)_2$, or a phase change between a largely disordered (but entirely amorphous for X-ray diffraction above 10.0 GPa (Fig. 1) and amorphous materials, occurs between 8.1 and 14.8 GPa. This is associated with the V–O bond length deformation of the VO_4^{3-} structural units. The lengthening of the V–O bonds could be related to the increase of the average coordination number of the V^{5+} cations in the amorphous material. However, the broad Raman bands at about 750 and 600 cm^{-1} due to the sixfold coordinated V atoms (19, 20, 26) are not visible in the collected spectra, although a broad spectral feature develops on the shoulder of the main V–O stretching band at about 790 cm^{-1}. This would suggest that even if there were a pressure-induced coordination change of the V atoms in amorphous $Ca_3(VO_4)_2$ at room temperature, the relative abundance of high-coordinated V atoms would not be high. The resemblance of the Raman spectra between 8.1 and 14.8 GPa to the spectra at lower pressures suggests that the amorphous (or largely disordered, but amorphous for X-ray diffraction) material in this pressure range still possesses a short-range

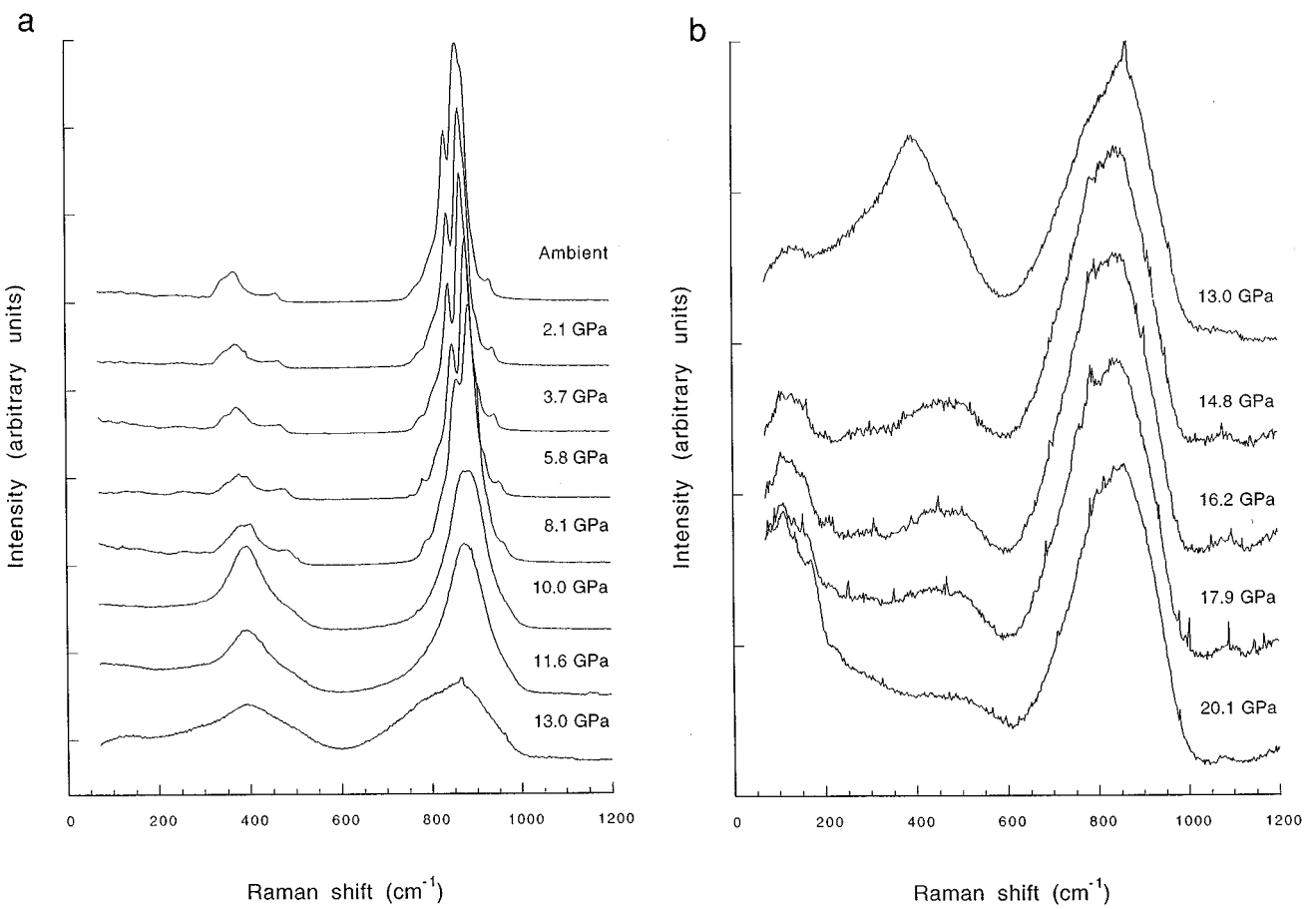

FIG. 4. Raman spectra of $Ca_3(VO_4)_2$ upon compression in the 0.0001- to 13.0-GPa (a) and 13.0- to 20.1-GPa (b) pressure ranges.

tetrahedral structure similar to the one in the parent crystalline phase.

Upon decompression, there is progressive sharpening of all the observed bands (Fig. 5). Whereas the bands in the 450- to 50-cm^{-1} region shift toward lower wavenumbers, the bands in the V–O stretching region do not shift significantly at all. The most remarkable change upon decompression is the decrease in intensity of the shoulder feature of the main V–O stretching band at about 790 cm^{-1}. This feature persists down to 9.3 GPa, showing a large hysteresis (about 6 GPa) of polymorphic phase changes within the amorphous $Ca_3(VO_4)_2$ material. The spectrum of the decompressed sample from 20.1 GPa still shows broad bands, very similar to the bands observed in the spectra upon compression at 8.1–14.8 GPa (Fig. 4).

The pressure dependence of the observed Raman bands up to 8.1 GPa can be correlated with the pressure dependence of the unit cell volume (Fig. 3 and Table 1) through a microscopic Grüneisen parameter (γ_i) at constant temperature, $T = 298$ K,

$$\gamma_i = (\partial \ln \nu_i / \ln V) = (K_0/\nu_i)\,(\partial \nu_i/\partial P),$$

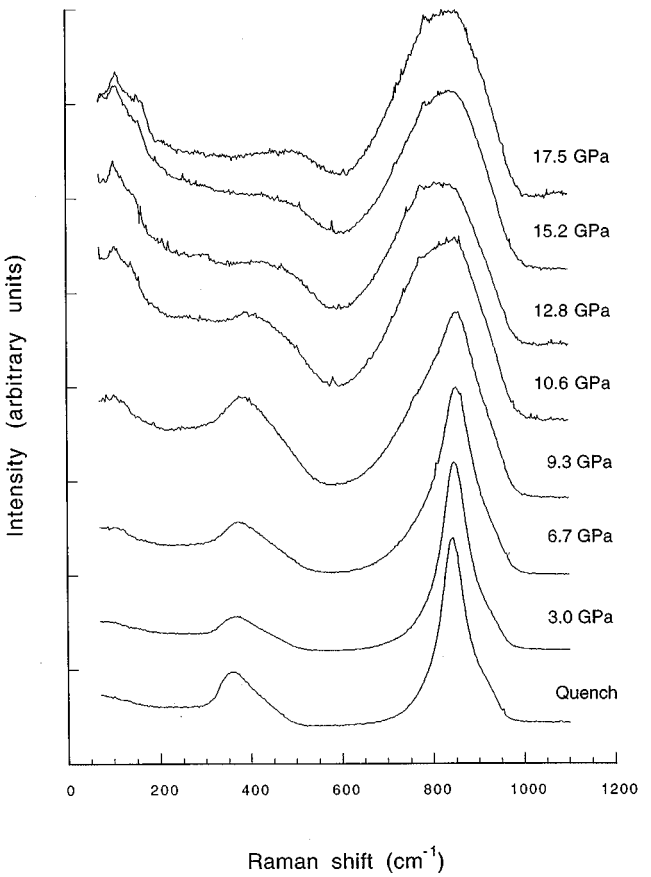

FIG. 5. Raman spectra of $Ca_3(VO_4)_2$ upon decompression.

where ν_i is the wavenumber of the ith vibrational mode (cm^{-1}), V is the corresponding unit cell volume ($Å^3$), K_0 is the isothermal bulk modulus at zero pressure (GPa), and P is the corresponding pressure (GPa). The resulting values of the $(\partial \nu_i/\partial P)$ (cm^{-1}/GPa) and γ_i parameters, using $K_0 =$ 92.5 GPa from the nonconstrained third-order Birch–Murnaghan equation of state (Table 1), are listed in Table 2.

Close examination of the calculated values of the microscopic Grüneisen parameters (Table 2) shows that their distribution corresponds to the distribution of the observed Raman bands in the two wavenumber regions corresponding to the V–O stretching modes (950–750 cm^{-1}) and the O–V–O bending modes mixed with the translational and rotational modes of the VO_4^{3-} groups as well as Ca^{2+} cation displacements (450–50 cm^{-1}). The Grüneisen parameters for the V–O stretching modes are similar to each other, with an average of 0.40 ± 0.06. The parameters corresponding to the modes in the 450- to 50-cm^{-1} wavenumber region are higher than this value and the differences among them are much larger. This observation could suggest, on the one hand, that any distortion of the $Ca_3(VO_4)_2$ lattice due to the decrease in volume of the unit cell up to about 8.0 GPa is associated with the O–V–O angles, VO_4^{3-} unit translational and rotational movements, and Ca atom displacements rather than with the V–O bond lengths. On the other hand, in the previous study on the high-pressure behavior of $Sr_3(VO_4)_2$, it was pointed out that the phase transition was due to the displacements of the $Sr^{2+}_{(2)}$ cations (20). Thus, the modes in crystalline $Ca_3(VO_4)_2$ with very large microscopic Grüneisen parameters (294, 220, 163, and 123 cm^{-1}) could be assigned mainly to the $Ca^{2+}_{(2)}$ displacements perpendicular to the c axis, along which the

TABLE 2
Observed Raman Bands in $Ca_3(VO_4)_2$ at Ambient Conditions and Their Pressure Dependence

ν (cm^{-1})	$(\partial\nu/\partial P)$(cm^{-1}/GPa)	γ
927	3.72	0.37
915	3.20	0.32
868	4.34	0.46
853	4.16	0.45
823	3.70	0.42
790	3.72	0.44
764	2.80	0.34
450	2.76	0.56
419	3.35	0.74
360	3.40	0.88
346	3.21	0.86
294	4.65	1.46
220	5.32	2.24
163	6.78	3.84
154	0.47	0.28
123	1.72	1.29
94	0.96	0.94

compressibility is much higher than the one along the *a* axis (Table 1). Such relative displacements of the interlayer cations should be strongly coupled with rotations of the VO_4^{3-} units.

DISCUSSION

The combined X-ray diffraction and Raman spectroscopy data show that $Ca_3(VO_4)_2$ irreversibly amorphizes at 10.0 GPa and room temperature. The amorphization, with its onset at about 8.5 GPa, is not preceded by any phase transition in the crystalline phase, which possesses highly anisotropic compressibility (the axial stiffness along the *a* axis in $Ca_3(VO_4)_2$ is over 30% larger than the axial stiffness along the *c* axis). The distortions of the lattice upon compression at the pressures up to the onset of amorphization are associated with the $Ca_{(2)}^{2+}$ cation displacements perpendicular to the *c* axis, strongly coupled with rigid rotations of the VO_4^{3-} units. Eventually, this leads to loss of long-range order and occurrence of the largely disordered (or amorphous for X-ray diffraction) phase, maintaining the tetrahedral short-range structure of the counterpart crystalline phase. The results of the Raman spectroscopy measurements demonstrate that further structural rearrangements in the amorphous $Ca_3(VO_4)_2$ occur between 8.1 and 14.8 GPa. This is associated with a large deformation of the VO_4^{3-} units or the increase of an average coordination number for the V^{5+} cations in the amorphous material. A large hysteresis of this phase change is observed upon decompression, pointing toward a first-order character of polymorphic transitions within the amorphous material. The recovered sample, after compression to 20.1 GPa, is amorphous with a structure similar to the short-range structure of crystalline $Ca_3(VO_4)_2$.

It was previously reported that $Ca_3(VO_4)_2$ synthesized at high pressure (5 GPa) and high temperature (1173 K) is monoclinic with a unit cell similar to that of the low-temperature monoclinic forms of $Pb_3(VO_4)_2$ (27, 28). This fact strongly indicates that the transformation between the $Ca_3(VO_4)_2$ and $Pb_3(VO_4)_2$-like structures is kinetically impeded at room temperature. In general, under pressure the low-density metastable phases tend to convert to denser stable phases and at high temperatures such reaction may actually occur. However, at low temperatures, the kinetics of this reaction may be very slow and the intermediate disorder could be frozen, yielding an amorphous state (29). In the case of $Ca_3(VO_4)_2$, this change to the thermodynamically stable but kinetically inaccessible $Pb_3(VO_4)_2$-like phase at high pressure and room temperature is not associated with mode softening, as demonstrated by Raman spectroscopy. The mechanism of this transformation would be similar to the one in $Pb_3(VO_4)_2$ at low temperatures (30, 32). The high-temperature γ form of $Pb_3(VO_4)_2$, with the ideal $R\bar{3}m$ palmierite structure, transforms into a monoclinic ferroelastic β phase ($P2_1/c$) and a ferroelectric α phase ($A2$) at 373 and 273 K, respectively. Through these transitions, not associated with a soft-mode behavior, the VO_4^{3-} tetrahedra remain rigid and the interlayer $Pb_{(2)}$ atoms are shifted from their ideal positions, perpendicular to the *c* axis. Recent studies of the phenomena due to the pressure-induced amorphization showed that the pressure–temperature phase diagrams of melts and amorphous materials are simplified and shifted phase diagrams of the corresponding crystalline phases (33). Thus, the presence of the polymorphic changes with large hysteresis on decompression in amorphous $Ca_3(VO_4)_2$ could be interpreted as an actual first-order phase transition, reflecting the tendency toward it in the high-pressure crystalline modifications in the approximate 10.0- to 15.0-GPa pressure range.

The high-pressure behavior of $Ca_3(VO_4)_2$ can be compared with pressure-induced structural changes in $Ba_3(VO_4)_2$ and $Sr_3(VO_4)_2$ (19, 20). Upon compression, the VO_4^{3-} units in $Ba_3(VO_4)_2$ condense into edge- or corner-shared octahedra with little or no hysteresis on decompression. For $Sr_3(VO_4)_2$, there is a pressure-induced first-order phase change at about 15.0 GPa, with large hysteresis on decompression. Thus, the high-pressure behavior of the compounds in the series $Ca_3(VO_4)_2$, $Sr_3(VO_4)_2$, and $Ba_3(VO_4)_2$ is related to the size of the $Me_{(2)}^{2+}$ cations. Small $Ca_{(2)}^{2+}$ cations hinder the completion of the transformation of $Ca_3(VO_4)_2$ into its high-pressure crystalline modifications.

ACKNOWLEDGMENTS

I thank Alain Polian and Paul McMillan for several suggestions and comments.

REFERENCES

1. A. M. Glass, S. C. Abrahams, A. A. Ballman, and G. Loiacono, *Ferroelectrics* **17,** 579 (1978).
2. S. Haussühl and J. Liebertz, *Z. Kristallogr.* **148,** 87 (1978).
3. A. A. Fotiev, B. K. Trunov, and V. D. Zhuravlev, "Vanadates of Divalent Metals" (in Russian). Nauka, Moscow, 1985.
4. M. Diouri, M. Drache, and D. Thomas, *Rev. Chim. Miner.* **23,** 746 (1986).
5. L. H. Brixner and P. A. Flournoy, *J. Electrochem. Soc.* **112,** 303 (1965).
6. M. Ya. Khodos, I. A. Leonidov, and A. A. Fotiev, *Russ. J. Inorg. Chem.* **29,** 1363 (1984).
7. C.-Z. Li, W.-H. Yang, and Y.-C. Chang, *Ferroelectrics* **142,** 131 (1993).
8. V. D. Zhuravlev, A. A. Fotiev, and B. V. Shulgin, *Izv. Akad. Nauk SSSR Neorg. Mater.* **15,** 2003 (1979).
9. L. D. Merkle, A. Pinto, H. Verdun, and B. McIntosh, *Appl. Phys. Lett.* **61,** 2386 (1992).
10. I. A. Leonidov, A. A. Fotiev, and M. Ya. Khodos, *Izv. Akad. Nauk SSSR Neorg. Mater.* **23,** 127 (1987).
11. I. A. Leonidov, M. Ya. Khodos, and A. A. Fotiev, *Izv. Akad. Nauk SSSR Neorg. Mater.* **24,** 97 (1988).
12. I. A. Leonidov, M. Ya. Khodos, A. A. Fotiev, and A. S. Zhukovskaya, *Izv. Akad. Nauk SSSR Neorg. Mater.* **24,** 347 (1988).
13. H. G. Bachmann and W. Kleber, *Fortschr. Mineral.* **31/32,** 9 (1953).

14. R. Gopal and C. Calvo, *Z. Kristallogr.* **137,** 67 (1973).
15. E. J. Baran, *Z. Anorg. Allg. Chem.* **427,** 131 (1976).
16. A. Durif, *Acta Crystallogr.* **12,** 420 (1959).
17. P. Tarte and I. Thelen, *Spectrochim. Acta, Part A*, **28,** 5 (1972).
18. E. J. Baran and P. J. Aymonino, *J. Mol. Struc.* **11,** 453 (1970).
19. A. Grzechnik and P. F. McMillan, *Solid State Commun.* **102,** 569 (1997).
20. A. Grzechnik and P. F. McMillan, *J. Solid State Chem.* **132,** 156 (1997).
21. P. Süsse and M. J. Buerger, *Z. Kristallogr.* **134,** 161 (1970).
22. W. Carrillo-Cabrera and H. G. von Schnering, *Z. Kristallogr.* **205,** 271 (1993).
23. H. K. Mao, P. M. Bell, J. W. Shaner, and D. J. Steinberg, *J. Appl. Phys.* **49,** 3276 (1978).
24. F. Birch, *J. Geophys. Res.* **83,** 1257 (1978).
25. A. Grzechnik, *Chem. Mater.*, **10,** 1034 (1998).
26. A. Grzechnik and P. F. McMillan, *J. Phys. Chem. Solids* **58,** 1071 (1997).
27. P. Roux and G. Bonel, *Bull. Mineral.* **107,** 635 (1984).
28. P. Roux and G. Bonel, *Rev. Chim. Miner.* **22,** 767 (1985).
29. E. G. Ponyatovsky and O. I. Barkalov, *Mater. Sci. Rep.* **8,** 147 (1992).
30. J. M. Kiat, P. Garnier, and M. Pinot, *J. Solid State Chem.* **91,** 339 (1991).
31. H. Kasatani, T. Umeki, and H. Terauchi, *J. Phys. Soc. Jpn.* **61,** 2309 (1992).
32. M. H. Kuok, S. C. Lee, S. H. Tong, M. Midorikawa, and Y. Ishibashi, *Solid State Commun.* **1988,** *66*, 1035.
33. V. V. Brazhkin, Programme of the Adriatico Research Conference, "Simple Systems at High Pressures and Temperatures: Theory and Experimets," Trieste, 1997.